Laser-written integrated platform for quantum storage of heralded single photons: supplementary material

A. SERI[1,*], G. CORRIELLI[2,*], D. LAGO-RIVERA[1], A. LENHARD[1], H. DE RIEDMATTEN[1,3], R. OSELLAME[2], AND M. MAZZERA[1,+]

[1]ICFO-Institut de Ciencies Fotoniques, The Barcelona Institute of Technology, 08860 Castelldefels (Barcelona), Spain
[2]Istituto di Fotonica e Nanotecnologie (IFN) - CNR and Dipartimento di Fisica - Politecnico di Milano, P.zza Leonardo da Vinci 32, 20133 Milano, Italia
[3]ICREA-Institució Catalana de Recerca i Estudis Avançats, 08015 Barcelona, Spain
*These authors contributed equally to this paper
+Corresponding author: margherita.mazzera@icfo.eu

This document provides supplementary informations to "Laser-written integrated platform for quantum storage of heralded single photons," https://doi.org/10.1364/OPTICA.5.000934.

In this supplementary material we report the details about the characterization of type I and type II waveguides, the experimental setup and the measurements performed to characterize the light matter interaction and the heralded single photon source used in the main paper.

1. WAVEGUIDES CHARACTERIZATION

In table S1 we list the values of the FWHM mode dimensions in the horizontal (Δ_H) and vertical (Δ_V) directions and the different contributions to losses for the type I and II waveguides presented in the main text.

From the values of $\Delta_{H,V}$ it is possible to appreciate that the type I waveguide supports a sensibly smaller mode than the type II ones. In addition, it is possible to see that Δ_H in type II waveguides strongly depends upon the distance d between the tracks, while Δ_V is almost unaffected by this parameter. This is consistent with the fact that the horizontal confinement in type II waveguides is provided by the high refractive index change of the core with respect to the lateral tracks, where the material becomes amorphous. The vertical confinement, instead, is given by the weak refractive index increase that occurs in the region between the tracks due to stress effects [1], and it is only barely influenced by d. In fact, the value of Δ_V is mainly determined by the vertical height of the laser-induced tracks, which measures approximately 20 μm. It is worth highlighting that the vertical extension of the tracks is a hardly controllable parameter during the fabrication of type II waveguides. It is, in fact, much longer than the confocal parameter of the focused laser beam inside the crystal, (around 4 μm in our case) and it is mainly determined by non-linear propagation effects (e.g. self focusing) caused by the very high optical power involved. A slight elongation in the vertical direction is visible also in type I waveguides, but in this case, as the writing power is sensibly smaller, it can be attributed mainly to the spherical aberrations of the focusing objective.

We performed the Insertion Losses (IL) measurement by coupling He-Ne light at λ=633 nm into the waveguides using a plano-convex lens with focal length f=75 mm, and collecting the light at the waveguide output with a microscope objective (40x, 0.65 NA). The laser beam impinging the lens was expanded to a $1/e^2$ diameter D_0=6 mm (circular cross section). This produces a FWHM focal spot size at the waveguide input facet equal to $\Delta_0 = 5.9$ μm. This value can be calculated by using the formula $\Delta_0 \approx 2.36 \cdot \lambda f / (\pi D_0)$, obtained from the theory of Gaussian beam focussing [2]. The value of IL in dB is calculated by the formula $\text{IL} = -10 \log_{10}(\text{P}_{\text{out}}/\text{P}_{\text{in}})$, where P_{in} and P_{out} are the light powers measured before and after the waveguides, respectively. This value comprises three distinct contributions: the coupling losses (CL) that arise from the mismatch between the focal spot and the waveguide modes, the Fresnel losses (FL) that are caused by reflection at the air/crystal interfaces, and the propagation losses (PL) caused by scattering of light from waveguide imperfections and by absorption of Pr^{3+}:Y_2SiO_5 at 633 nm along propagation. We estimated the values of CL by calculating numerically the superposition integral η between the field distribution at the focal spot $E_{\text{IN}} = \exp[-1.39(x^2 + y^2)/\Delta_0^2]$ and that of the waveguides mode $E_{\text{WG}} = \exp[-1.39(x^2/\Delta_H^2 + y^2/\Delta_V^2)]$,

WG Type	d (μm)	Δ_{H} (μm)	Δ_{V} (μm)	IL (dB)	CL (dB)	FL (dB)	PL (dB/cm)
I	-	3.1	5.9	1.8	0.84	0.37	1.6
II	10	5.0	12.1	12.0	1.09	0.37	28.5
II	12.5	6.1	12.5	7.0	1.12	0.37	14.9
II	15	7.2	12.5	4.3	1.21	0.37	7.4
II	17.5	8.6	12.0	2.8	1.31	0.37	3.0
II	20	9.9	12.5	2.4	1.68	0.37	0.9

Table S1. Summary of the results obtained from the characterization of the type I and II laser written waveguides presented in the main text. d is the distance between the side tracks of type II waveguides, $\Delta_{H/V}$ are the FWHM horizontal/vertical dimensions of the guided mode, IL stands for Insertion Losses, CL stands for Coupling Losses, FL stands for Fresnel Losses and PL stands for Propagation Losses.

as defined in [3]. The value reported in table S1 is then calculated as CL $= -10 \log_{10}(\eta)$. The single-interface FL are calculated as FL $= -10 \log_{10}(1 - r)$, where r is the Fresnel reflection coefficient obtained considering $n_c = 1.8$ for the Pr^{3+}:Y_2SiO_5 refractive index. Finally, PL are calculated as PL $= (IL - CL - FL)/L_c$, where L_c=3.7 mm is the crystal length. In this formula FL are counted only once, because an anti-reflection coating is present on the crystal input facet. It is worth noting that, despite the significant difference in mode dimensions between the waveguides, the variation in CL is rather limited when compared to the variation observed for IL. As a consequence, the IL trend presented in fig. 1(b) of the main text can be almost entirely ascribed to the different values of PL. In the case of type type II waveguides PL are highly affected by the scattering due to the roughness of the side tracks, and this effect becomes more and more relevant for decreasing values of d. The quasi-periodic damages that affect type II waveguides (visible as black spots in fig. 1(c) of the main text) along the writing direction can be explained by thermal accumulation processes that cause quasi-periodic micro-explosions in the material. They are particularly relevant for type II waveguides where the pulse energy is much higher, while they are not present in type I waveguides. A similar phenomenon has been already observed and explained for FLM in fused silica [4].

2. EXPERIMENTAL SETUP

The experimental setup for the spectroscopic characterization of the waveguides and single photon storage measurements is sketched in fig. 2 of the main text. We hereby provide a more detailed description. Our laser source at 606 nm is a Toptica DL SHG pro, frequency stabilized using the Pound-Drever-Hall technique to a home-made Fabry-Perot cavity placed in a vacuum chamber. We estimate the final laser linewidth to be about 20 kHz. The CW laser light is modulated in amplitude and frequency with acousto-optic modulators (AOMs) in double-pass configuration, driven by an arbitrary waveform generator (Signadyne). The preparation light is coupled into one input of a fiber beam splitter (BS, input 1 in fig. 2 in the main text). In input 2 we send the input for the storage (either classical pulses or heralded single photons, see below). One output is sent to an independent optical table where the Pr^{3+}:Y_2SiO_5 crystal (Scientific Materials) with laser written waveguides is maintained at 3 K (in a He closed cycle cryocooler, Oxford Instrument), while the second output is used as reference. The light is coupled into the waveguide using a 75 mm lens, which focuses the beam to a

waist $< 10\,\mu$m at the input facet of the crystal. The out coming light from the waveguide is collected with a 50 mm lens and sent to a detection stage, after a path of about 2 m. It is worth noting that both lenses are placed outside of the cryostat chamber, thus making the alignment of the whole system rather challenging. The detection is implemented with a CCD camera, for imaging and alignment, with a photo-detector, for protocols with classical light, or with a single photon detector (SPD) for experiments with single photons.
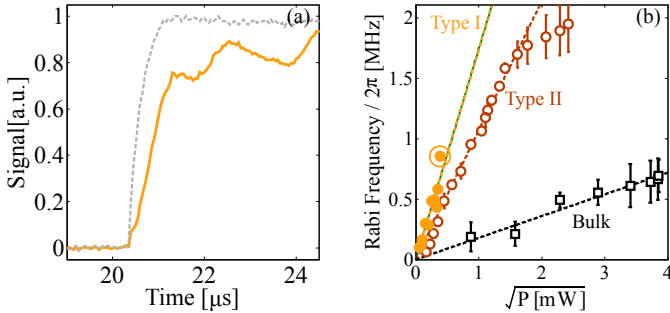
All the experiments are synchronized with the cycle of the cryostat (1.4 Hz) to reduce the effect of the mechanical vibrations. Two mechanical shutters are installed in the setup during the single photon measurements: one, in front of the SPD, remains closed during the preparation period; the second, in anti-phase with the first one, is installed before the input 1 of the fiber BS, and remains closed during the single photon measurement period, blocking the leakage from the preparation AOM. The SPD is a Laser Components detector with 50% detection efficiency and 10 Hz dark-count rate. For unconditional and heralded auto-correlation measurements the waveguide output is split with a fiber BS and an Excelitas SPD with 50% detection efficiency and 50 Hz dark-count rate is connected to the second output.

Our heralded single photons are generated with a photon pair source (fig. 2 of main text) inspired by the source described in [5]. It is based on cavity-enhanced spontaneous parametric down-conversion process (SPDC) in a 2 cm-long type I periodically-poled lithium niobate (PPLN). The non-linear crystal is pumped with a 426 nm laser (Toptica TA SHG) to produce signal photons at 606 nm and idler photons at 1436 nm. The crystal is placed inside a bow-tie cavity (BTC) with a free spectral range (FSR) of 261 MHz to enhance the generation of the photon pairs at the frequencies of the cavity modes. The BTC is maintained in resonance to both the signal and its heralding idler photon at 1436 nm with a double lock system. First of all, the cavity length is locked using the Pound-Drever-Hall technique to a reference beam at 606 nm derived from the main memory preparation laser [5]. Then, a classical beam at 1436 nm, generated as frequency difference (DFG) of the pump and the reference beam at 606 nm, is used to ensure the maximum transmission of the idler photons through the BTC. The lock of the DFG signal is operated by acting on the 426 nm pump frequency. Two mechanical choppers are used to alternate between the locking period and the single-photon measurement. The BTC, besides enhancing the non-linear process at the two resonant wavelengths, is meant to generate ultra narrow-band photons [5]. A consequence of

the double lock is the clustering effect given by the different FSR at the signal and idler frequencies [9]. This results in a spectral output of the SPDC source consisting of a main cluster with only 8 effective spectral modes separated by 261 MHz. The photons of the pair are generated collinearly and separated after the BTC using a dichroic mirror (DM, fig. 2 in the main text). The idler photon passes through a home-made Fabry-Perot filter cavity (FC in fig. 2 of the main text, linewidth 80 MHz, FSR=17 GHz), to guarantee a single-spectral-mode heralding. It is then coupled into a single mode fiber to an SPD (ID230, IDQuantique), with 10% efficiency and 10 Hz of dark-count rate. For the auto-correlation measurement of the idler photons, we use a second SPD (ID220, IDQuantique), with 10% efficiency and 400 Hz of dark-count rate. The 606 nm photons then pass through an etalon (linewidth 4.25 GHz, FSR=100 GHz) that suppresses the side clusters. Finally they are coupled in a single-mode polarization-maintaining (PM) fiber and then to the input 2 of the fiber BS. The heralding efficiency of the SPDC source is $\eta_H^{\mathrm{SPDC}} \sim 25\%$ after the PM fiber and $\eta_H^{\mathrm{WG}} \sim 7\%$ in front of the waveguide.

3. LIGHT-MATTER INTERACTION

The interaction between light and matter is highly enhanced in the waveguide, thanks to the high confinement of the light through the whole length of the crystal. We quantify the strength of this interaction measuring the Rabi frequency Ω_R, by means of optical nutation [7]: we prepare by optical-pumping a single-class absorption feature on the $1/2g - 3/2e$ transition and measure the population inversion time t_π induced by a long resonant probe pulse (grey dashed trace in fig. S1(a)). For a Gaussian beam in an optically dense and inhomogeneously broadened ensemble, the Rabi frequency Ω_R is defined as $\Omega_R t_\pi = 5.1$ [7].
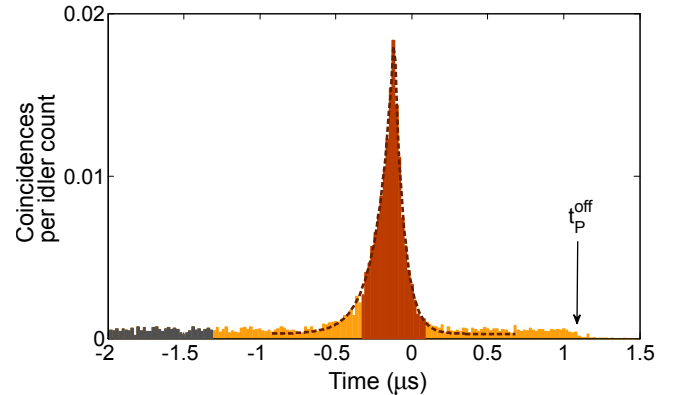

Fig. S1. (a) The solid orange trace is the measured intensity of a long light pulse, $P = 0.51$mW, transmitted by a single-class absorption feature on the $1/2g - 3/2e$ transition. The gray dotted line is the reference pulse before entering the crystal. (b) Rabi frequency as a function of the pulse power as calculated from optical nutation measurements performed on the waveguide type I (filled orange circles), compared with the Ω_R measured in a longer bulk sample (empty black squares) containing also a type II waveguide (empty brown circles) [6]. The dashed lines are the linear fits of the experimental data. The green solid line is the expected behavior for the type I waveguide from the slope of the type II fit, scaled according to the different diameters. The circled data point in panel (b) refers to the pulse reported in panel (a).

We repeat the measurement for several probe powers, P (orange filled points in fig. S1(b)). We show in fig. S1(b), for comparison, the measured Ω_R for different P in a waveguide

type II and in bulk (respectively brown empty circles and black empty squares), from our previous work in a longer sample [6], being the dotted lines fits of the data. From the linear fit of Ω_R vs $\sqrt{P}$ for the type I (orange dotted line), we extract $\Omega_R = 2\pi \times 1.75\,\mathrm{MHz}/\sqrt{\mathrm{mW}}$. This value agrees quite well with that calculated from the dipole moment of the investigated transition (1.45×10^{-32} Cm [8]), i.e. $2\pi \times 1.6\,\mathrm{MHz}/\sqrt{\mathrm{mW}}$. For this calculation we consider a Gaussian mode with the average FWHM diameter measured at 606 nm with the same setup used for the optical nutation measurements. In this condition, the measured diameters (4.5 μm and 7.6 μm in the horizontal and vertical directions, respectively) are slightly different than those quoted in section 1, as the two setups differ in many aspects, e.g. the light wavelength, the objective and CCD camera. The Rabi frequency measured for the type I waveguides features an increase of 1.6 with respect to the previously measured type II waveguide and almost one order of magnitude with respect to the bulk crystal [6]. This result fully matches with the expected increase due to the stronger light confinement, green solid line below the fit, which has been calculated from the fit of the type II (brown dotted line), renormalized for the different mode diameter in the waveguide type I.

4. CHARACTERIZATION OF THE HERALDED SINGLE PHOTONS

Before sending the signal photons through the fiber BS and to the memory setup, we directly connect the output of the source to the SPD, to measure the properties of the generated heralded single photons. We record the detection times of both signal and idler photons with a fast time-stamping electronics (Signadyne).
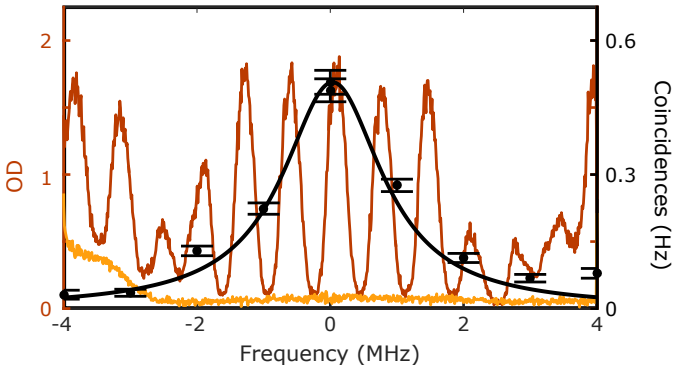

Fig. S2. Time-resolved coincidence histogram between the two photons, the darker orange region being the signal-of-interest and the gray region on the left being the accidental coincidences considered for the calculation of the $g_{s,i}^{(2)}$ (400 ns window). The black dashed line is the temporal fit of the biphoton correlation. The arrow points at the gating off of the pump laser to the photon pair source.

Then we build a time-resolved coincidence histogram, using the idler detections as start and the signal photons as stop (fig. S2). The correlation time of our biphoton can be estimated by fitting the histogram with two exponential decays [5] (black dotted lines on top of the histogram). The two decay times are different due to the different losses experienced in the cavity by the signal and the idler photons, generated at widely different frequencies.

From the right (left) decay we can extract the linewidth of the signal (idler) photons to be $\Gamma_s = 2.5\,\text{MHz}$ ($\Gamma_i = 1.4\,\text{MHz}$). The resulting biphoton linewidth is $\Gamma = 1.8\,\text{MHz}$ in FWHM (equivalent to a coherence time of 121 ns), narrow enough to address a single transition of Pr^{3+} ions.

To confirm the linewidth of the correlations, we use the crystal as a tunable ultranarrow spectral filter, following a measurement described in [10]: we hole-burn a transparency window (*pit*), centered each time at a different frequency around the signal photons, and we analyze the change in the coincidence rate after it. To prepare a *pit* we shine the crystal with strong pulses at the desired frequency and with a frequency chirp dependent on the width of the *pit* that we want to create, in this case $\sim 1.6\,\text{MHz}$. The coupling optics is free-space and outside the cryostat (see sect. 2). Inside the cryostat is only the waveguide which moves periodically with injection of compressed liquid He in the cooling device (cooling period 707 ms), thus the light is effectively coupled in the waveguide for a time $< 300\,\text{ms}$. Having fiber coupled samples would relax the time limitation and enable better optical pumping. We *reset* the absorption spectrum and prepare the *pit* at the beginning of each cycle, limiting our measurement duty cycle to $\sim 30\%$. Having fiber-coupled devices would allow us to increase significantly the duty cycle of the experiment. The coincidence rates for *pit*s prepared at different frequencies are plotted in the inset of figure 5 of the main paper (black dots), which is reported here (fig. S3). The black line, a Lorentzian function with a linewidth of $\Gamma = 1.8\,\text{MHz}$ in FWHM, convoluted with the spectral trace of the *pit*, matches with the measured data. This confirms the linewidth estimated from the coincidence histogram (fig. S2).

Fig. S3. Absorption profiles of the *pit* (orange) and the comb (brown). The black line represents the spectral shape of the heralded single photons, a Lorentzian function of 1.8 MHz bandwidth, convoluted with the trace of the *pit* used as tunable filter. The black dots are the coincidence rate of the heralded signal photons passing through the waveguide used as a tunable filter centered at different frequencies.

We quantify the non-classicality of the photon-pair correlations measuring the normalized second-order cross-correlation function: $g_{s,i}^{(2)}(\Delta t) = p_{s,i}/(p_s \cdot p_i)$, where $p_{s,i}$ is the probability to detect a coincidence in a temporal window Δt, while p_s (p_i) is the probability to detect a signal (idler) count in a temporal window of the same size. The $g_{s,i}^{(2)}$ is extracted from the coincidence histogram of figure S2, by integrating the coincidence counts in a window Δt around the coincidence peak (our signal of interest $p_{s,i}$, dark orange region of the histogram) and dividing them by the coincidences outside of it (accidental coincidences between

uncorrelated photons or detector dark counts, $p_s \cdot p_i$, gray region of the histogram) [5], renormalized to a window Δt. We integrate the counts over a window $\Delta t = 400\,\text{ns}$. The measured $g_{s,i}^{(2)}$ values for different pump powers are plotted in figure 4a of the main paper (empty orange circles).

This measurement alone does not demonstrate the quantum nature of our correlations, which can be shown by violating the Cauchy-Schwartz (CS) inequality. The classical bound is given by the parameter $R = \frac{(g_{s,i}^{(2)})^2}{g_{s,s}^{(2)} \cdot g_{i,i}^{(2)}} \leq 1$, where $g_{s,s}^{(2)}$ ($g_{i,i}^{(2)}$) is the auto-correlation of the signal (idler) photons. We measure the unconditional auto-correlation of the signal (idler) photon by splitting its path with a fiber BS and detecting the two outputs with two different SPDs. From the resulting coincidence histogram we extract the auto-correlation value (similarly to the cross-correlation measurement). Using an integration window $\Delta t = 400\,\text{ns}$ for comparison with the $g_{s,i}^{(2)}$, we find $g_{s,s}^{(2)}(400\,\text{ns}) = 1.051 \pm 0.002$ and $g_{i,i}^{(2)}(400\,\text{ns}) = 1.25 \pm 0.03$. The expected auto-correlation for an ideal state generated by a photon source with thermal statistics is $g_{x,x}^{(2)\,th}(0) = 2$ [11]. As the signal photons, measured without any filter cavity, are multi-mode and knowing that we have a number of frequency modes N = 8, we expect for the signal photons $g_{s,s}^{(2)\,th}(0) = 1 + 1/N = 1.12$ [12]. Anyway the auto-correlation values of both idler and signal photons are lower than expected because we measured them in a 400 ns window (instead of extracting their values in the 0-point) and because the noise generated by the source reduces the auto-correlation value (a detailed discussion can be found in [5]).

Using these values, we find for the lowest pump power $R = (3.3 \pm 0.3) \times 10^4$, surpassing the classical bound by more than 10 standard deviations. Even for the highest pump power (2 mW), where the measured cross-correlation is $g_{s,i}^{(2)}(400\,\text{ns}) = 13.8 \pm 0.3$, we find $R = 145 \pm 6$, which violates the CS inequality by more than 20 standard deviations, thanks to the better statistics.

To demonstrate the single photon nature of our source, we measure the heralded auto-correlation $g_{i:s,s}^{(2)}(\Delta t)$: the auto-correlation of the signal is measured conditioned on the detection of an heralding in the same integration window Δt. The histogram of figure 4b of the main paper, inspired from [13], is built as follows: for each count in the idler detector we look for detection events in the two signal detectors, happening in the same temporal window ($\Delta t = 400\,\text{ns}$ around the heralding). If there is a count in one of the two signal lists, we look for the closest event in the other one. The triple-coincidences are then sorted depending on the number of heralding events between each two contiguous signal detections. The events in which a coincidence between the two signal detectors is heralded by the same idler count are plotted in the bin 0. The ratio between the counts in bin 0 and the average of the other bins (black dotted line in figure 4b of the main paper) gives the heralded auto-correlation, which we measure to be $g_{i:s,s}^{(2)}(400\,\text{ns}) = 0.12 \pm 0.01$ (pump power $\sim 1.7\,\text{mW}$). This value is considerably lower than the classical bound $g_{i:s,s}^{(2)} \geq 1$ and compatible with the single photon behavior ($g_{i:s,s}^{(2)} \leq 0.5$).

5. CHARACTERIZATION OF THE HERALDED SINGLE PHOTONS AFTER THE *PIT*

We connect the signal photons fiber output to the input 2 of the fiber BS and we couple them into the waveguide, as sketched in

the setup (figure 2 of the main paper).

We hole-burn a *pit* of $\sim 16\,\text{MHz}$ in the inhomogeneously broadened absorption profile of the ions (the spectral trace of the *pit* in OD is plotted as an orange line in figure S3). We measure the $g_{s,i}^{(2)}$ between the heralding photons and the signal photons passing through the *pit* similarly to the previous section. The results, measured for different powers in the same range of the measurement with just the source, are plotted in figure 4a of the main paper (full brown circles). The non-classicality of the correlations after the *pit* is remarkably higher than the one of the source alone. For example, the $g_{s,i}^{(2)}$ at the highest pump power (2 mW) is found to be 36 ± 3, being almost three times higher than the $g_{s,i}^{(2)}$ of the source alone. This can be explained by a spectral filtering effect of the *pit*. The spectral modes in the signal arm that do not have an heralding photon and are not filtered by the etalon (see section 2) are in fact absorbed by the atoms outside of the *pit*. Due to the low count-rate, caused by transmission losses as well as short measurement duty-cycle, we do not have enough statistics in the auto-correlation measurement of the signal after the *pit* (an exploratory trace more than 20 h long does not show any bunching). We consider the conservative value of 2 for an ideal two-mode squeezed state for the signal [11] and the measured value only for the idler photons, leading to a classical bound of $\sqrt{g_{s,s}^{(2)} \cdot g_{i,i}^{(2)}} = 1.58 \pm 0.02$. Even with this assumptions we find $R = 524 \pm 84$ after the *pit* for the highest measured power, violating the CS inequality by more than 6 standard deviations.

Finally, we measure the heralded auto-correlation of the signal photons after the *pit*: the signals are sent through the crystal, then split with a fiber BS and detected with two different SPDs. From the post-processed histogram (fig. 4c of the main paper) we extract $g_{i:s,s}^{(2)}(400\,\text{ns}) = 0.06 \pm 0.04$ (pump power $\sim 1.7\,\text{mW}$). We know that the $g_{i:s,s}^{(2)}$ is inversely proportional to $g_{s,i}^{(2)}$ for two-mode squeezed states and low pump powers [14]. This is verified in our measurement, in fact the heralded auto-correlation is lower after the *pit*, where the cross-correlation is higher. For a pump power of 1.7 mW, using $g_{s,s}^{(2)} = 2$ and the measured value for $g_{i,i}^{(2)}$, we find $g_{i:s,s}^{(2)\,\text{th}} = g_{s,s}^{(2)} \cdot g_{i,i}^{(2)}/g_{s,i}^{(2)} \sim 0.06$ which matches with the measured heralded auto-correlation.

REFERENCES

1. T. Gorelik, M. Will, S. Nolte, A. Tuennermann and U. Glatzel, "Transmission electron microscopy studies of femtosecond laser induced modifications in quartz," Appl. Phys. A **76**, 309 (2003).
2. O. Svelto and D. C. Hanna, *Principles of Lasers* (Springer, 1998).
3. R. Osellame, N. Chiodo, G. Della Valle, S. Taccheo, R. Ramponi, G. Cerullo, U. Morgner, M. Lederer and D. Kopf, "Optical waveguide writing with diode-pumped femtosecond oscillator," Opt. Lett. **29**, 1900 (2004).
4. S. Richter, S. Döring, F. Burmeister, A. Tünnermann and S. Nolte, "Formation of periodic disruptions induced by heat accumulation of femtosecond laser pulses," Opt. Express **21**, 15452 (2013).
5. D. Rieländer, A. Lenhard, M. Mazzera, and H. de Riedmatten, "Cavity enhanced telecom heralded single photons for spin-wave solid state quantum memories," New Journal of Physics **18**, 123013 (2016).
6. G. Corrielli, A. Seri, M. Mazzera, R. Osellame, and H. de Riedmatten, "Integrated optical memory based on laser-written waveguides," Physical Review Applied **5**, 054013 (2016).
7. Y. Sun, G. M. Wang, R. L. Cone, R. W. Equall, and M. J. M. Leask, "Symmetry considerations regarding light propagation and light polarization for coherent interactions with ions in crystals," Phys. Rev. B **62**, 15443 (2000).
8. M. Nilsson, L. Rippe, S. Kröll, R. Klieber, and D. Suter, "Hole-burning techniques for isolation and study of individual hyperfine transitions in inhomogeneously broadened solids demonstrated in Pr^{3+}:Y_2SiO_5," Phys. Rev. B **70**, 214116 (2005).
9. E. Pomarico, B. Sanguinetti, C. I. Osorio, H. Herrmann, and R. T. Thew, "Engineering integrated pure narrow-band photon sources," New Journal of Physics **14**, 33008 (2012).
10. A. Seri, A. Lenhard, D. Rieländer, M. Gündoğan, P. M. Ledingham, M. Mazzera, and H. de Riedmatten, "Quantum correlations between single telecom photons and a multimode on-demand solid-state quantum memory," Phys. Rev. X **7**, 021028 (2017).
11. P. R. Tapster and J. G. Rarity, "Photon statistics of pulsed parametric light," Journal of Modern Optics **45**, 595 (1998).
12. K. J. McNeil and C. W. Gardiner, "Quantum statistics of parametric oscillation," Phys. Rev. A **28**, 1560 (1983).
13. S. Fasel, O. Alibart, S. Tanzilli, P. Baldi, A. Beveratos, N. Gisin, and H. Zbinden, "High-quality asynchronous heralded single-photon source at telecom wavelength," New Journal of Physics **6**, 163 (2004).
14. C. W. Chou, S. V. Polyakov, A. Kuzmich, and H. J. Kimble, "Single-Photon Generation from Stored Excitation in an Atomic Ensemble," Phys. Rev. Lett. **92**, 213601 (2004).